APL Photonics

Invited Article: Optical dynamic range compression

Cite as: APL Photonics **3**, 110806 (2018); https://doi.org/10.1063/1.5051566
Submitted: 10 August 2018 • Accepted: 06 October 2018 • Published Online: 14 November 2018

Yunshan Jiang, Saili Zhao and Bahram Jalali

Invited Article: Optical dynamic range compression

Yunshan Jiang,[1,a] Saili Zhao,[1] and Bahram Jalali[1,2,3,4]
[1]*Department of Electrical and Computer Engineering, University of California, Los Angeles, California 90095, USA*
[2]*Department of Bioengineering, University of California, Los Angeles, California 90095, USA*
[3]*Department of Surgery, David Geffen School of Medicine, University of California, Los Angeles, California 90095, USA*
[4]*California NanoSystems Institute, Los Angeles, California 90095, USA*

(Received 10 August 2018; accepted 6 October 2018; published online 14 November 2018)

We introduce the concept of optical dynamic range compression and discuss its utilities in the non-uniform quantization, enhancing the signal-to-noise ratio as well as reshaping signal's statistical distribution and extending the detection range in light detection and ranging systems. The technology represents a photonics hardware accelerator that reduces the burden on the dynamic range of the photodetection and the data acquisition including the required number of bits of the analog-to-digital converter. The energy of photons that are intentionally blocked can be harvested using a two-photon photovoltaic effect. Implementations using other approaches are also discussed. https://doi.org/10.1063/1.5051566

I. INTRODUCTION

A detector with a large dynamic range is desired in nearly all optical sensing and communication applications, including ranging,[1] spectroscopy,[2,3] fluorescence imaging,[4–7] optical coherent tomography,[8] quantum optics,[9] and coherent optical networks.[10] For example, in Light Detection and Ranging (LiDAR) systems, the power of the returned signal decays quadratically with the distance so that the maximum detection range is limited by the dynamic range of the detection.

The trade-off between speed, sensitivity, and dynamic range poses fundamental challenges to the detection system. Optical amplifiers boost the lower portion of the dynamic range above the noise floor and help with the measurement of small signal amplitudes. However, it also requires the receiver to have a larger linear range and a higher number of bits for quantization.[11] Optical detectors with the internal amplification (e.g., avalanche photodiodes) are used for sensitive measurements of faint light, whereas the detection speed is limited by the fundamental trade-off between the gain and the bandwidth in all electronic systems.[12] While averaging reduces the effective noise and increases the sensitivity, it inevitably reduces the speed.

Photonic hardware accelerators are analog optical processors that promise to alleviate bottlenecks associated with the digital acquisition and processing of optical data.[13–15] One example is the amplified photonic time-stretch technology that performs the optical analog slow-motion processing and overcomes the speed-sensitivity trade-off in time-resolved single-shot measurements.[16] Here we propose another type of photonic hardware accelerator—the optical dynamic range compressor (ODRC). It is a new optical signal processing method that tackles the trade-off between sensitivity and dynamic range in high-speed optical signal detection.

This relieves the requirement on the dynamic range of the photoreceiver and the number of bits of analog-to-digital converters (ADCs). The concept is illustrated in Fig. 1. The analog optical signal is first reshaped by the optical dynamic range compressor through the logarithmic-like transform.

[a]Electronic mail: yunshanjiang@gmail.com

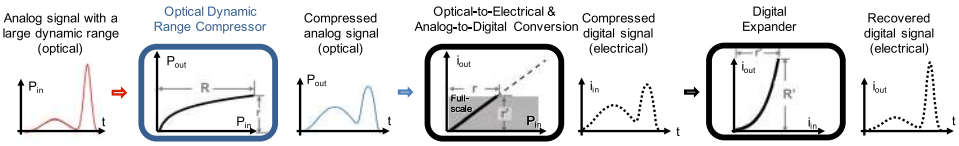

FIG. 1. Diagram of the optical dynamic range compression. The dynamic range of the input optical signal is compressed in the optical dynamic range compressor, whose gain changes dynamically as a logarithmic-like function of the instantaneous input power. After the optical-to-electrical conversion by the photoreceiver and the analog-to-digital-conversion by the digitizer, the compressed signal is recovered through the digital expander whose response is the inverse of that of the optical compressor.

The optical transformation reduces the large dynamic range of the input to match that of the detecting system. After the optical-to-electrical and the analog-to-digital conversion, the compressed digital signal is recovered through the digital expander whose response is the inverse function of that of the optical compressor. Without requiring an optical receiver with a larger dynamic range or more quantization bits, the detectable range is extended.

The paper is arranged as follows. First, we explain the improvements on the detection sensitivity in the presence of different types of noises. Then, we show the impact of ODRC on signal statistics and LiDAR systems. Finally, we discuss the realization of ODRC and demonstrate transform profiles changing from smooth compression to sharp compression by exploring the nonlinear propagation in nano-scale silicon waveguides.

II. IMPROVEMENT ON DETECTION SENSITIVITY

The dynamic range of a detecting system is the difference between the smallest and the largest signal value (full-scale) it can measure. The smallest measurable signal is determined by the signal-independent noises in the detection, such as the thermal noise, dark noise, and quantization noise (for quantization, the peak signal is matched to the full-scale of the ADC). The largest measurable signal is limited by the saturation of the photodiode during the optical-to-electrical conversion and the clipping by the quantizer during the analog-to-digital conversion.

A. Dynamic range limits

We now discuss the dynamic range limits imposed by the photodiode, optical amplifier, and quantizer in the high-speed optical signal detection.

The ratio between the saturation limit and the input-referred noise floor depicts the dynamic range of a photoreceiver.[17] In detecting very weak inputs, the inevitable noise that originates from the thermal motion of electrons in the load resistor dominates the receiver performance (assuming photodiodes with a low dark current). At high level optical input, the output of a photodiode begins to deviate from the linear response, as evidenced by a reduction in the output current and by a diminished bandwidth. This is primarily attributed to the space-charge effect that leads to the reduction in carrier velocities and a corresponding build-up of carriers.[18,19]

A linear optical amplifier is able to boost the signal above the thermal noise of the photoreceiver and improve the sensitivity. Optical amplifiers are used when the receiver is thermal noise limited. On the other hand, since the maximum level is also increased by the same ratio, the upper range of the signal will exceed the detector saturation and the dynamic range of the ADC.

The most significant challenge with optical measurements is the trade-off between the dynamic range [measured in the effective number of bits (ENOBs)] and the speed of the ADC.[20–23] While the thermal noise is the major limit at low speeds, the ambiguity caused by the limited gain bandwidth of transistors and the clock jitter becomes the dominant limitation at high frequencies.

ODRC can mitigate the burden on the saturation of photodetectors and the dynamic range of the ADCs. It provides a gain that decreases as the signal amplitude increases, improving the detection sensitivity without saturating the full-scale, as shown in Fig. 2. The output signal P_{out} after ODRC can be written as

$$P_{out} = g(P_{in}) \cdot P_{in}. \tag{1}$$

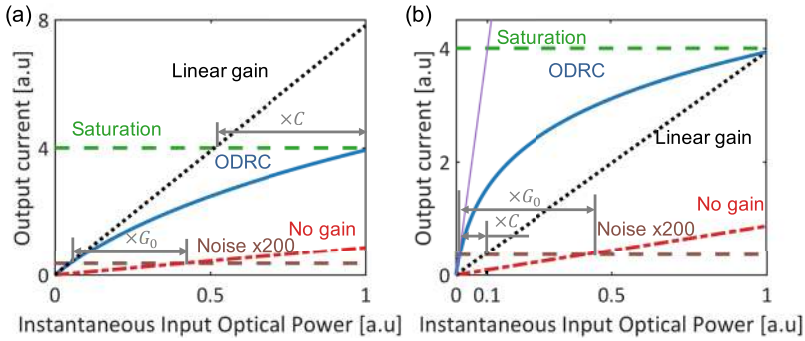

FIG. 2. ODRC mitigates the burden on the dynamic range of the detection system. The signal-independent detection noise (brown dashed line), such as the thermal noise, dark noise, and quantization noise, determines the minimum measurable signal. The saturation of the photodiode and the ADC (green dashed line) determine the maximum input. Linear amplifier (black dotted line) boosts the signal above the noise level with the unwanted effect of a smaller maximum input. ODRC (blue solid curve) tackles the trade-off by providing a logarithmic-type gain that decreases as the instantaneous input optical power increases. (a) As compared to a linear amplifier with the same small signal gain G_0, ODRC compresses the upper range. The maximum input level is increased by a ratio of the compression factor $C = 2$. (b) As compared to a linear amplifier with the same gain at the maximum input level, ODRC provides a higher gain for the lower range (the small gain is shown as the purple thin line). The detection sensitivity is improved by a ratio of the compression factor $C = 10$. The logarithmic-type compression is obtained using the nonlinear propagation in silicon with nonlinear losses and saturated Raman amplification. Similar behavior can be achieved with other types of amplifiers (with fast gain response) (see Fig. 7).

Here $g(P_{in})$ is the logarithmic-like gain of the input signal P_{in}. Here, P_{out} is a monotonically increasing concave function of P_{in}. The small signal gain G_0 is calculated as

$$G_0 = \lim_{P_{in}\to 0} \frac{P_{out}}{P_{in}} = g(0). \tag{2}$$

And the compression ratio C at input P_{in} is defined as the ratio between the small signal gain and the gain at input P_{in},

$$C(P_{in}) = \frac{G_0}{g(P_{in})}. \tag{3}$$

The compression ratio depicts the curvature of the sublinear gain profile. The larger it is, the more compression the signal undergoes.

B. Improvement over ADC quantization noise

Performing ODRC on the optical signal before the photodetection and A/D conversion leads to the non-uniform quantization where the quantization step increases as a function of the input signal amplitude. This highly desired transformation is shown in Fig. 3. Compared to the linear case, the lower portion of the dynamic range is quantized with higher resolution, at the expense of the accuracy of the upper portion. The latter is acceptable because the impact of quantization noise is much more severe at low signal levels.

The mean square quantization error or quantization noise power of an ideal ADC is calculated as[24,25]

$$\sigma_q^2 = E\left[(x - Q(x))^2\right] = \int_{-\infty}^{\infty} (x - Q(x))^2 p(x)dx = \sum_{k=1}^{2^n} \int_{b_{k-1}}^{b_k} (x - y_k)^2 p(x)dx, \tag{4}$$

where x is the input signal, $Q: x \to y_k, \forall x \in [b_{k-1}, b_k)$ is the mapping function of quantization, $p(x)$ is the probability density function of the input x, and n is the nominal number of the bits of the ADC. When the quantization step $\Delta_k = b_k - b_{k-1}$ is small enough and the threshold value is set as the median of the bin $[y_k = (b_{k-1} + b_k)/2]$, (4) can be approximated as

$$\sigma_q^2 \approx \sum_{k=1}^{2^n} \int_{-\frac{\Delta_k}{2}}^{\frac{\Delta_k}{2}} x^2 p(x)dx \approx \frac{1}{12} \sum_{k=1}^{2^n} \Delta_k^2 \cdot \Pr(P_{in}), \tag{5}$$

where $\Pr(P_{in}) = \int_{b_{k-1}}^{b_k} p(x)dx$ is the probability of the input falling in a given quantization bin.

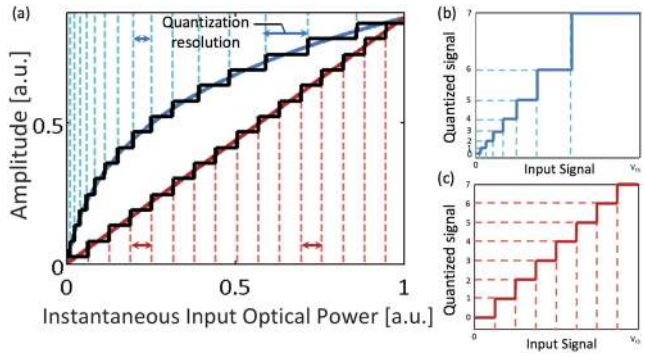

FIG. 3. ODRC enables the non-uniform quantization where the quantization step increases as a function of the input signal amplitude. Compared to the linear case, the lower part of the dynamic range is associated with the finer quantization resolution, at the expense of the accuracy of the upper part. The latter is acceptable because the impact of quantization noise is much more severe at low signal levels. (a) The photocurrent in the case of ODRC (blue) and linear (red) transformation is quantized with a uniform ADC (black). Quantization steps are illustrated in dashed vertical lines. The mapping between the analog input signal to the quantized digital output in the case of ODRC is shown in (b) and in the case of the linear transformation is shown in (c). In (b), the quantized signal is recovered through the digital expander whose response is the inverse of that of the optical compressor.

In the case of a uniform quantizer, the quantization resolution is a function of the full-scale V_{FS} and the nominal number of bits, n, and is independent of signal's instantaneous amplitudes,

$$\Delta_{linear} = \frac{V_{FS}}{2^n}. \tag{6}$$

When the probability of the input falling in each interval is the same, a uniform quantizer minimizes the quantization noise power. Inserting (6) into (5) results in the well-known equation for the quantization error,

$$\sigma_q^2 = \frac{\Delta_{linear}^2}{12}. \tag{7}$$

ADC's dynamic range is defined as the ratio of its full-scale range to the minimum resolvable change in signal. For a linear quantizer, it is proportional to the bit number n,

$$DR_{ADC}\,(\mathrm{dB}) = 20\,\log\left(\frac{V_{FS}}{\Delta_{linear}}\right) = 6.02n. \tag{8}$$

Note that (8) differs from the formulation of the ADC's signal-to-noise ratio (SNR) equation by 1.76 dB, since the latter is in terms of root-mean-square values, whereas the former is for peak-to-peak amplitudes. When detecting inputs with a large dynamic range, one needs to determine the proper balance between the large amplitudes, which exceed ADC's full-scale, and the small amplitudes, which get lost in quantization noise.

ODRC tackles this trade-off by boosting the small amplitude without exceeding the full-scale. The quantization resolution is a function of the input amplitude

$$\Delta_{ODRC}(P_{in}) = \frac{\Delta_{linear}}{\mathrm{d}P_{out}/\mathrm{d}P_{in}} = \frac{V_{FS}/2^n}{g'(P_{in}) * P_{in} + g(P_{in})}. \tag{9}$$

The dynamic range enhancement of an ADC is

$$DR_{ADC}\,(\mathrm{dB}) = 20\,\log\left(\frac{V_{FS} \times C(P_{max})}{\Delta_{linear}}\right) = 6.02n + 20\,\log(C(P_{max})). \tag{10}$$

Therefore, the dynamic range is improved by $20\log(C(P_{max}))$, where $C(P_{max})$ is the compression factor that is evaluated at the maximum input P_{max} which does not saturate the full-scale.

The reshaping of quantization noise is shown in Fig. 4. The lower portion of the dynamic range is quantized with smaller noise, resulting in a higher signal-to-noise ratio (SNR). This is obtained at the expense of a decreased SNR at the higher portion of the dynamic range. As compared to the

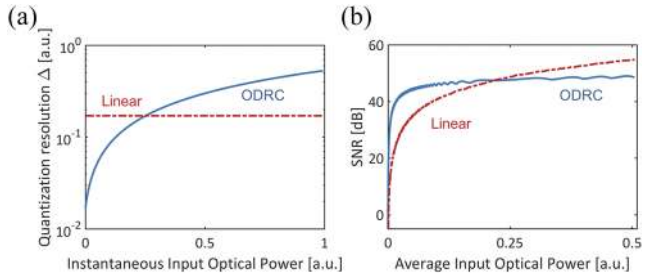

FIG. 4. ODRC reshapes the quantization noise. The lower portion of the dynamic range is quantized with less noise and better SNR, at the expense of decreased SNR at the higher portion. (a) The quantization resolution as a function of the input amplitude. (b) Signal-to-quantization-noise ratio of quantizing a single-tone input with an 8-bit linear ADC. (The full-scale of the ADC is matched to the maximum input peak.) As compared to the case of the linear quantization (red dotted-dashed curve), where the SNR falls rapidly for small amplitudes, ODRC (blue solid curve) is able to provide good SNR over a wide range of signal powers. ODRC that is considered here has a compression factor C = 10.

case in the linear quantization, where the SNR falls rapidly for small amplitudes, ODRC is able to provide the good SNR over a wide range of signal levels.

Inserting (9) into (5), the mean square quantization error is calculated as

$$\sigma_q^2 \approx \frac{1}{12}\sum_{k=1}^{2^n}\left(\frac{V_{FS}/2^n}{g'(P_{in}) * P_{in} + g(P_{in})}\right)^2 \Pr(P_{in}). \tag{11}$$

Given the signal statistics described by its probability distribution function $\Pr(P_{in})$, there exists the optimal nonlinear transform $g(P_{in})$ that minimizes the expectation of the quantization error. To achieve the same digital SNR, the signal that is optically compressed requires fewer bits than otherwise required by a linear converter. This powerful idea enables the non-uniform quantization and data compression to be performed in the optical domain.

For input signals with a non-stationary probability distribution, the sublinear transform of the optical compressor can be dynamically adapted to the histogram of the input amplitudes. The idea can be applied to smart sensing, providing flexible solutions to meet the requirements on the resolution and the accuracy in optical detections and analog-to-digital conversions.

III. EXTENDING DETECTION RANGE OF LiDAR

LiDAR systems measure the distance and velocity of targets by illuminating the target and measuring the time-of-flight and Doppler shift of the reflected light. The power of the returned signal decays quadratically with the distance. As a result, the maximum detection range is limited by the dynamic range of the detection and the analog-to-digital converter, characterized by the digitizer's effective number of bits (ENOBs). Thus high-resolution (high-ENOB) ADCs are required in the LiDAR system to achieve a large detection range. In the meantime, the depth accuracy of the system is limited by the sampling speed of the digitizer that decreases with ENOBs.

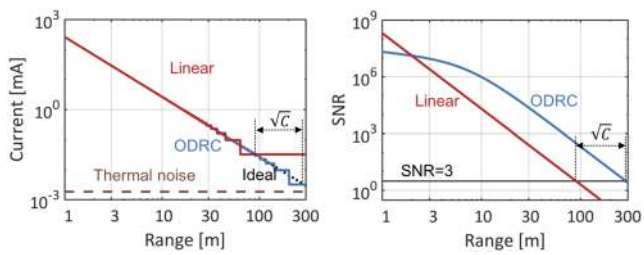

FIG. 5. ODRC extends the detection range of LiDAR. Weak signals from distant targets are quantized with finer steps after reshaping by ODRC. The maximum detection range, which scales quadratically with the measured amplitude, is improved by the square root of the compression factor $\sqrt{C}$.

ODRC extends the detection range of LiDAR systems by assigning more quantization bits (improving ENOBs) for weak signals and lowering the minimum returned power the ADC can quantize, as shown in Fig. 5. As compared to the linear case, the SNR for detecting distant targets is increased. The maximum detection range, which scales quadratically with the measured amplitude, is improved by the square root of the compression factor, $\sqrt{C}$.

IV. SHAPING SIGNAL STATISTICS

ODRC redistributes statistics of a signal. By amplifying small amplitudes and compressing large amplitudes, ODRC causes a relative compression in the right side of the distribution with a concomitant suppression of outlier events.

While the Gaussian distribution is widely used to model noise in optical systems, the extreme-value statistics that studies the rare events has drawn much attention in the past decade.[26–28] In stimulated Raman amplification, extreme-value behaviors arise due to the interplay of pump laser fluctuations with the exponential transfer function of the Raman process. Studies have shown that the amplified Stokes signal has a heavy-tailed distribution.[26] The effect of ODRC on the extreme-value statistics is shown in Fig. 6. ODRC compresses the heavy tail in the high-value region and mitigates the burden on the receiving system for detecting high-dynamic-range inputs, facilitating the study of extreme events in nonlinear optical systems.

Optical dynamic range compression may reduce the nonlinear phase noise (NLPN). NLPN is caused by the interaction of amplitude fluctuations, such as amplified spontaneous noise (ASE) and relative intensity noise (RIN), with self-phase modulation (SPM). By suppressing large-amplitude events in the probability distribution, ODRC can reduce the nonlinear phase noise.

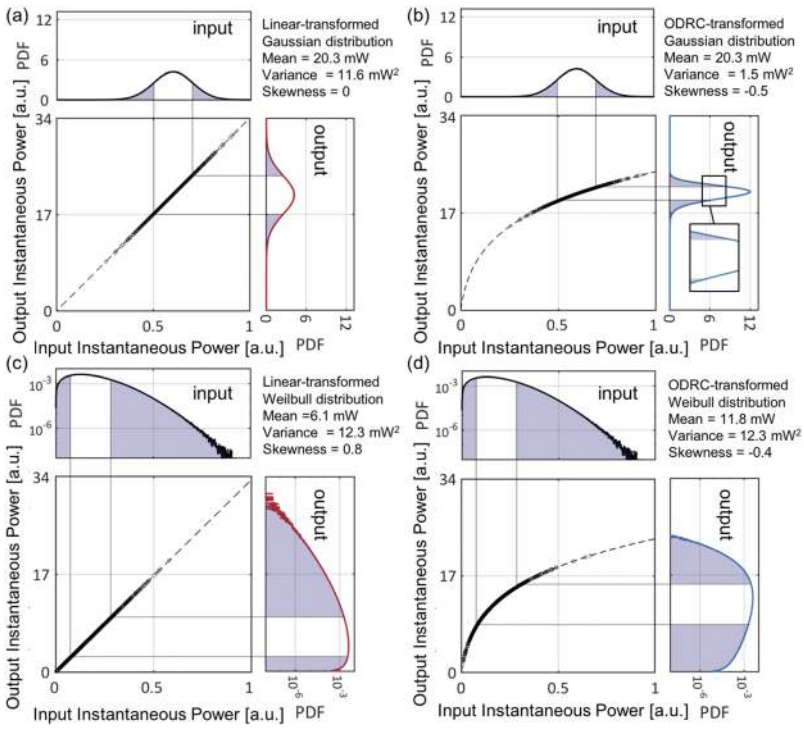

FIG. 6. ODRC reshapes signal statistics including noise characteristics. [(a) and (b)] ODRC reshapes the statistics of a Gaussian-distributed signal. As compared to a linear amplifier with the same average gain, it reduces the variance and the skewness of the signal (as shown by the asymmetric distribution in the subset), resulting in improved SNR. [(c) and (d)] ODRC reshapes the statistics of a signal that follows the extreme-value distribution, shown in the logarithmic scale here. As compared to the linear amplifier that preserves the shape of the distribution, ODRC reduces the requirement for a large dynamic range in optical detection and A/D conversion stages of a receiver.

V. PHYSICAL REALIZATION OF ODRC

Owing to the logarithmic current-to-voltage transfer characteristic inherent in PN-junctions, logarithmic compressors are widely implemented in electronics. They are used in radar and radio applications to compress the high dynamic range of received signals at MHz.[29] Due to the lack of logarithmic behaviors in optics, implementing such powerful techniques optically has not been possible.

Recently, an optical method to create the logarithmic function was introduced. The saturated amplification and nonlinear absorption in a silicon photonics waveguide were tailored to approximate a logarithmic function with an input range of up to 19.5 dB. The optical logarithm was shown to perform optical exponentiation and signal deconvolution.[30,31] This opens one possible path to realize the dynamic range compression optically. Fortunately, an exact logarithmic behavior is not needed for ODRC, making the implementation easier.

Various approaches for the experimental realization of ODRC are illustrated in Fig. 7. To compress the high-dynamic-range-optical signals in high-speed detection, ODRC devices should have a nonlinear gain/loss that decreases/increases as input amplitudes increase, and should be able to respond to the instantaneous power change.

Saturated amplifiers can be used to shape input amplitudes by providing a higher gain for small inputs, and a lower gain for large inputs as the pump is depleted. This behavior can be tuned by changing the pump power. A stronger pump leads to a larger compression ratio. Amplifiers with ion-doped gain medium such as erbium-doped fiber amplifier (EDFA) and ytterbium-doped fiber amplifier (YDFA) have gain relaxation time at milliseconds owing to the long metastable lifetime. Such a long relaxation time is preferable for low noise but also limits the device's response time. Semiconductor optical amplifiers (SOA), on the other hand, have a much shorter upper state lifetime of few nanoseconds. Saturated SOAs can also be used to compress signals. The lifetime of SOA can be dramatically reduced to pico-seconds with quantum-dot structures.[32]

Raman amplification that is based on stimulated Raman scattering (SRS) is widely used in optical communications and biomedical applications for its broadband gain and low noise performance. The response time of the Raman process is at the order of tens of femtoseconds in amorphous solids such as glasses, and a few pico-seconds in crystalline solids such as silicon.[33,34] For ODRC using Raman-pumped optical fibers of kilometers, the walk-off between the co-propagating pump and signal beams becomes the major limitation of the device bandwidth.[35] Raman amplification has a gain coefficient in silicon that is four orders larger than it is in silica[36] and it was used to realize the first silicon optical amplifier[37] and the first silicon laser.[34] Unlike the SOA, Raman amplification causes minimum phase distortions and can be used for ODRC in coherent applications.

Two-photon absorption (TPA) generates loss that increases quadratically with the input intensity and can be used to compress high amplitudes at ultrafast speed. In semiconductors like silicon, free carriers generated during TPA introduce free carrier absorption (FCA) that contributes to dynamic range compression. However, the free carriers with a long lifetime reduce the response speed.[38] Studies have also shown that TPA-induced free-carrier loss degrades the noise figure of a silicon Raman amplifier by an amount that depends on the carrier lifetime.[39] The silicon nanowire usage can greatly enhance the nonlinear effect as well as increase the device bandwidth and reduce the noise figure, as the intensity increases and lifetime reduces in nanoscale waveguides.[40] The carrier

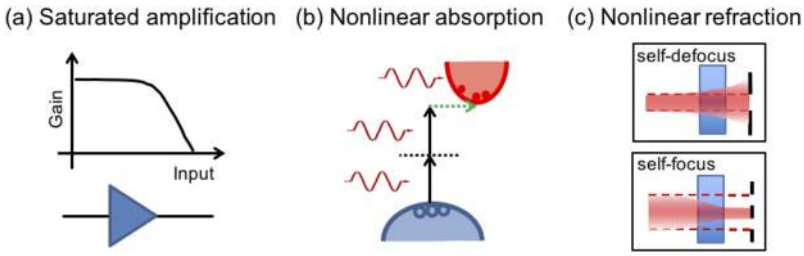

FIG. 7. Various approaches for the experimental realization of ODRC.

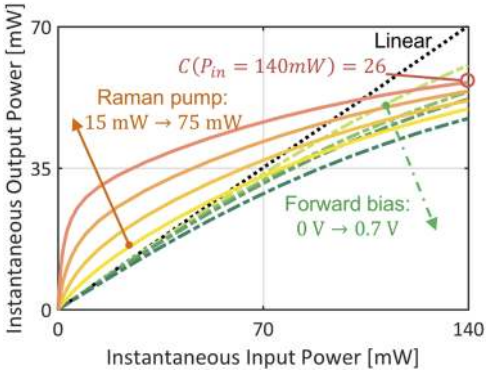

FIG. 8. ODRC with energy harvesting is realized in a forward-biased nano-scale silicon waveguide with saturated Raman amplification. A tunable compression profile is achieved by varying Raman pump intensity and forward bias. When forward bias increases from 0 V to 0.7 V and Raman pump is 0 mW (line's color varies from light green to dark green), more free carriers generated from TPA can accumulate in the waveguide, resulting in a more compressed output. When Raman pump increases from 15 mW to 75 mW and forward bias is 0.7 V (line's color varies from yellow to red), gain depletes at weaker input. A sharp compression profile is realized using large Raman pump and high forward bias. The compression factor at 140 mW input is 26 with 75 mW Raman pump and 0.7 V forward bias (waveguide dimension: 220 nm*450 nm*1 cm).

sweep-out using a reverse-biased PN-junction further reduces the free-carrier lifetime to tens picoseconds.[36,41] III-V materials, such as GaAs and InP, are also candidates for performing ODRC. They have a two-photon absorption coefficient much larger than that of silicon, and a short lifetime as a result of the direct bandgap.[42,43]

While the reverse-biased waveguide enables carrier removal and ODRC at high operation bandwidth, a forward-biased waveguide can be used to harvest the energy during the compression at the cost of device speed.[44] Here, using the two-photon photovoltaic (TPPV) effect, electric power is recycled from the photons that were lost through the compression of the high amplitudes. Energy harvesting has been achieved in silicon wavelength converters,[45] modulators,[46] and Raman amplifiers.[47] Such low-energy consumption devices reduce power dissipation as well as chip heating, which are of paramount importance for chip-scale integration in silicon photonics.

We demonstrate ODRC with energy harvesting by simulation of the nonlinear propagation in a forward-biased nano-scale silicon waveguide, taking saturated Raman amplification, TPA, and FCA into account. Logarithmic-transform profiles with soft and sharp compression are achieved by varying the input Raman pump intensity and the bias voltage, as shown in Fig. 8. A tunable ODRC allows one to select the optimal compression profile that matches with signal statistics, adaptively balance between the detection of small and large amplitudes, maximizing the detection SNR. ODRC

TABLE I. Potential implementations of ODRC.

Device	Power consumption	Speed (GHz)	Compression ratio	Noise figure (dB)	Principles	Complexity
Reverse-biased silicon nanowire with saturated Raman pump	Medium	>50[38]	Large and tunable	~5[39]	SRS, TPA, FCA	Medium
Optical fiber with saturated Raman pump	High	>1[35]	Large and tunable	~5[52]	SRS	Medium
Saturated SOA	Medium	>1	Large and tunable	~8	SOA	Medium
Forward-biased silicon nanowire	Negative[44]	>0.5[38]	Medium	>3	TPA, FCA, TPPV	Medium
GaAs resonator	Zero	>1[49]	Medium	>3	TPA, FCR, FCA	Medium
Quantum-well-based optical limiter	Zero	>50[51]	Large	>3	Optical Kerr	High

devices based on nonlinear absorption has an operation wavelength limited by material bandgap. For wavelength above 2.2 μm, nonlinear absorption will not be an option for compression due to the absence of TPA, and only saturated amplification can be utilized.[48]

Nonlinear refraction mechanisms form another approach for the experimental realization of ODRC. In nonlinear materials, the large peaks produce changes in the refractive index that lead to an intensity-dependent loss in the transmission.[49,50] For example, a positive/negative lens generated by the strong inputs causes the beam to self-focus/self-defocus and to be blocked by an aperture placed at the output.[51] This non-absorptive phenomenon can realize compression with a large compression factor. It can be cascaded with the saturated amplification and nonlinear absorption to construct versatile ODRC devices. The proposed methods for the experimental realization of ODRC are compared in Table I.

VI. CONCLUSIONS

We describe a new concept in optical signal processing that can improve the sensitivity and dynamic range, and outline several methods for its experimental realization. The nonlinear optical transformations utilized here increase the signal bandwidth, which is potentially an undesired effect. Therefore, they should be utilized only when the system is dynamic-range-limited and not bandwidth-limited. Time stretch techniques have been very successful in overcoming the bandwidth limitation in optical data acquisition and have led to spectacular successes in the discovery of new optical phenomena and creation of a new class of biomedical instruments with extreme throughput.[15] Combining time stretch with optical data compression presents an intriguing area for research.

ACKNOWLEDGMENTS

This work was supported in part by the Office of Naval Research (ONR) MURI Program on Near-Field Nanophotonics for Energy Efficient Computing and Communication (NECom).

[1] B. Lienert, J. Porter, N. Ahlquist, D. Harris, and S. Sharma, "A 50-MHz logarithmic amplifier for use in Lidar measurements," J. Atmos. Oceanic Technol. **19**(5), 654–657 (2002).
[2] A. Dalla Mora, A. Tosi, F. Zappa, S. Cova, D. Contini, A. Pifferi, L. Spinelli, A. Torricelli, and R. Cubeddu, "Fast-gated single-photon avalanche diode for wide dynamic range near infrared spectroscopy," IEEE J. Sel. Top. Quantum Electron. **16**(4), 1023–1030 (2010).
[3] J. Chou, Y. Han, and B. Jalali, "Time-wavelength spectroscopy for chemical sensing," IEEE Photonics Technol. Lett. **16**(4), 1140–1142 (2004).
[4] E. Diebold, B. Buckley, D. Gossett, and B. Jalali, "Digitally synthesized beat frequency multiplexing for sub-millisecond fluorescence microscopy," Nat. Photonics **7**(10), 806 (2013).
[5] C. Vinegoni, C. L. Swisher, P. F. Feruglio, R. J. Giedt, D. L. Rousso, S. Stapleton, and R. Weissleder, "Real-time high dynamic range laser scanning microscopy," Nat. Commun. **7**, 11077 (2016).
[6] H. C. Gerritsen, M. A. Asselbergs, A. V. Agronskaia, and W. G. Van Sark, "Fluorescence lifetime imaging in scanning microscopes: Acquisition speed, photon economy and lifetime resolution," J. Microsc. **206**(3), 218–224 (2002).
[7] M. Eibl, S. Karpf, D. Weng, H. Hakert, T. Pfeiffer, J. P. Kolb, and R. Huber, "Single pulse two photon fluorescence lifetime imaging (SP-FLIM) with MHz pixel rate," Biomed. Opt. Express **8**, 3132–3142 (2017).
[8] Q. Tang, Y. Liu, V. Tsytsarev, J. Lin, B. Wang, U. Kanniyappan, Z. Li, and Y. Chen, "High-dynamic-range fluorescence laminar optical tomography (HDR-FLOT)," Biomed. Opt. Express **8**, 2124–2137 (2017).
[9] J. Tiedau, E. Meyer-scott, T. Nitsche, S. Barkhofen, C. Silberhorn, and T. J. Bartley, "Measuring single photons to bright light with a logarithmic optical detector," in *Conference on Lasers and Electro-Optics* (Optical Society of America, 2018), pp. 6–7.
[10] Y. Shen, N. C. Harris, S. Skirlo, M. Prabhu, T. Baehr-Jones, M. Hochberg, X. Sun, S. Zhao, H. Larochelle, D. Englund, and M. Soljačić, "Deep learning with coherent nanophotonic circuits," Nat. Photonics **11**, 441–446 (2017).
[11] A. Mahjoubfar, K. Goda, G. Betts, and B. Jalali, "Optically amplified detection for biomedical sensing and imaging," J. Opt. Soc. Am. A **30**(10), 2124–2132 (2013).
[12] M. Nada, T. Hoshi, H. Yamazaki, T. Hashimoto, and H. Matsuzaki, "Linearity improvement of high-speed avalanche photodiodes using thin depleted absorber operating with higher order modulation format," Opt. Express **23**(21), 27715–27723 (2015).
[13] D. Solli and B. Jalali, "Analog optical computing," Nat. Photonics **9**(11), 704–706 (2015).
[14] F. Coppinger, S. Yegnanarayanan, P. Trinh, and B. Jalali, "All-optical incoherent negative taps for photonic signal processing," Electron. Lett. **33**(11), 973–975 (1997).
[15] F. Coppinger, A. S. Bhushan, and B. Jalali, "Time magnification of electrical signals using chirped optical pulses," Electron. Lett. **34**(4), 399–400 (1998).

[16] A. Mahjoubfar, D. V. Churkin, S. Barland, N. Broderick, S. K. Turitsyn, and B. Jalali, "Time stretch and its applications," Nat. Photonics **11**(6), 341–351 (2017).
[17] L. Naval, B. Jalali, L. Gomelsky, and J. M. Liu, "Optimization of $Si_{1-x}Ge_x$/Si waveguide photodetectors operating at $\lambda = 1.3\ \mu$m," J. Lightwave Technol. **14**(5), 787–797 (1996).
[18] P. Liu, K. J. Williams, M. Y. Frankel, and R. D. Esman, "Saturation characteristics of fast photodetectors," IEEE Trans. Microwave Theory Tech. **47**(7), 1297–1303 (1999).
[19] D. Dimitropoulos, S. Fathpour, and B. Jalali, "Limitations of active carrier removal in silicon Raman amplifiers and lasers," Appl. Phys. Lett. **87**(26), 261108 (2005).
[20] R. H. Walden, "Analog-to-digital converter survey and analysis," IEEE J. Sel. Areas Commun. **17**(4), 539–550 (1999).
[21] B. Jalali, D. R. Solli, K. Goda, K. Tsia, and C. Ropers, "Real-time measurements, rare events and photon economics," Eur. Phys. J.: Spec. Top. **185**(1), 145–157 (2010).
[22] B. Murmann, "ADC performance survey 1997-2015," http://web.stanford.edu/~murmann/adcsurvey.html.
[23] J. Chan, A. Mahjoubfar, M. Asghari, and B. Jalali, "Reconstruction in time-bandwidth compression systems," Appl. Phys. Lett. **105**(22), 221105 (2014).
[24] R. M. Gray and D. L. Neuhoff, "Quantization," IEEE Trans. Inf. Theory **44**(6), 2325–2383 (1998).
[25] B. Smith, "Instantaneous companding of quantized signals," Bell Syst. Tech. J. **36**(3), 653–709 (1957).
[26] D. R. Solli, C. Ropers, P. Koonath, and B. Jalali, "Optical rogue waves," Nature **450**(7172), 1054–1057 (2007).
[27] P. T. S. DeVore, D. R. Solli, D. Borlaug, C. Ropers, and B. Jalali, "Rogue events and noise shaping in nonlinear silicon photonics," J. Opt. **15**(6), 064001 (2013).
[28] D. Borlaug, S. Fathpour, and B. Jalali, "Extreme value statistics in silicon photonics," IEEE Photonics J. **1**(1), 33–39 (2009).
[29] See http://www.ti.com/amplifier-circuit/special-function/logarithmic/products.html for Logarithmic Amplifiers, Texas Instruments.
[30] Y. Jiang, P. DeVore, and B. Jalali, "Analog optical computing primitives in silicon photonics," Opt. Lett. **41**(6), 1273–1276 (2016).
[31] Y. Jiang, P. DeVore, A. Mahjoubfar, and B. Jalali, "Signal de-convolution with analog logarithmic computing primitives in silicon photonics," in *Photonics Society Summer Topical Meeting Series (SUM)* (IEEE, 2016), pp. 70–71.
[32] M. Sugawara, H. Ebe, N. Hatori, M. Ishida, Y. Arakawa, T. Akiyama, K. Otsubo, and Y. Nakata, "Theory of optical signal amplification and processing by quantum-dot semiconductor optical amplifiers," Phys. Rev. B **69**(23), 235332 (2004).
[33] J. Liu, *Photonic Devices* (Cambridge University Press, 2009).
[34] O. Boyraz and B. Jalali, "Demonstration of a silicon Raman laser," Opt. Express **12**(21), 5269–5273 (2004).
[35] C. R. S. Fludger, V. Handerek, and R. J. Mears, "Pump to signal RIN transfer in Raman fiber amplifiers," J. Lightwave Technol. **19**(8), 1140 (2001).
[36] B. Jalali and S. Fathpour, "Silicon photonics," J. Lightwave Technol. **24**(12), 4600–4615 (2006).
[37] R. Claps, D. Dimitropoulos, V. Raghunathan, Y. Han, and B. Jalali, "Observation of stimulated Raman amplification in silicon waveguides," Opt. Express **11**(15), 1731–1739 (2003).
[38] X. Sang, D. Dimitropoulos, B. Jalali, and O. Boyraz, "Influence of pump-to-signal RIN transfer on noise figure in silicon Raman amplifiers," IEEE Photonics Technol. Lett. **20**(24), 2021–2023 (2008).
[39] D. Dimitropoulos, D. R. Solli, R. Claps, O. Boyraz, and B. Jalali, "Noise figure of silicon Raman amplifiers," J. Lightwave Technol. **26**(7), 847–852 (2008).
[40] D. Dimitropoulos, R. Jhaveri, R. Claps, J. C. S. Woo, and B. Jalali, "Lifetime of photogenerated carriers in silicon-on-insulator rib waveguides," Appl. Phys. Lett. **86**(7), 071115 (2005).
[41] A. Turner-Foster, M. Foster, J. Levy, C. Poitras, R. Salem, A. Gaeta, and M. Lipson, "Ultrashort free-carrier lifetime in low-loss silicon nanowaveguides," Opt. Express **18**(4), 3582–3591 (2010).
[42] B. Jalali and S. J. Pearton, *InP HBTs: Growth, Processing, and Applications* (Artech House Publishers, 1995).
[43] J. Ma, J. Chiles, Y. D. Sharma, S. Krishna, and S. Fathpour, "Two-photon photovoltaic effect in gallium arsenide," Opt. Lett. **39**(18), 5297–5300 (2014).
[44] S. Fathpour, K. Tsia, and B. Jalali, "Two-photon photovoltaic effect in silicon," IEEE J. Quantum Electron. **43**(12), 1211–1217 (2007).
[45] K. Tsia, S. Fathpour, and B. Jalali, "Energy harvesting in silicon wavelength converters," Opt. Express **14**(25), 12327–12333 (2006).
[46] S. Fathpour and B. Jalali, "Energy harvesting in silicon optical modulators," Opt. Express **14**(22), 10795–10799 (2006).
[47] S. Fathpour, K. K. Tsia, and B. Jalali, "Energy harvesting in silicon Raman amplifiers," Appl. Phys. Lett. **89**(6), 061109 (2006).
[48] V. Raghunathan, D. Borlaug, R. R. Rice, and B. Jalali, "Demonstration of a mid-infrared silicon Raman amplifier," Opt. Express **15**(22), 14355–14362 (2007).
[49] L. Tutt and T. Boggess, "A review of optical limiting mechanisms and devices using organics, fullerenes, semiconductors and other materials," Prog. Quantum Electron. **17**, 299–338 (1993).
[50] Y. Xiao, H. Qian, and Z. Liu, "Nonlinear metasurface based on giant optical Kerr response of gold quantum wells," ACS Photonics **5**(5), 1654–1659 (2018).
[51] H. Qian, Y. Xiao, and Z. Liu, "Giant Kerr response of ultrathin gold films from quantum size effect," Nat. Commun. **7**, 13153 (2016).
[52] J. Bromage, "Raman amplification for fiber communications systems," J. Lightwave Technol. **22**(1), 79 (2004).